Supplementary Material

Development and assessment of speed-up algorithms for the reactive CFD-DEM simulation of fluidized bed reactors

Riccardo Uglietti[a], Mauro Bracconi[a], Matteo Maestri[a]*

[a]Laboratory of Catalysis and Catalytic Processes, Dipartimento di Energia, Politecnico di Milano via La Masa 34, 20156 Milano, Italy

*corresponding author: matteo.maestri@polimi.it (M. Maestri)

1 Reactive CFD-DEM framework

The fluidized bed is updated at each time step by solving sequentially the solid and the gas phases in the reactor.

1.1 Solid Phase

The solid phase is updated particle-wise considering the gas phase frozen. Each pellet composing the fluidized bed is tracked through the computational grid, which is fixed and particle-independent. The particle tracking is performed by solving the momentum and angular momentum balances on the catalytic pellet. Moreover, the ODE system, composed by the species mass, species sites and energy balances, is integrated for each catalytic pellet. In particular, the model of the particle neglects intra-particle gradients thanks to the fine size of the particles adopted in this technology.

The momentum (Eq.(S1)) and angular momentum balances (Eq.(S2)) on each particle are reported as follows:

$$\frac{d\boldsymbol{v}_p}{dt} = \frac{\boldsymbol{F}_{d,p} + \boldsymbol{F}_{b,p} + \boldsymbol{F}_{coll,p}}{m_p} + \boldsymbol{g} \qquad \textbf{(S1)}$$

$$\frac{d\boldsymbol{w}_p}{dt} = \frac{\sum[R_p \boldsymbol{n} \wedge \boldsymbol{F}_{coll,p}]}{I_p} \qquad \textbf{(S2)}$$

where m, I, **v**, **w** are the mass, the moment of inertia, the velocity and angular velocity of the *p*th particle, $\boldsymbol{F}_{coll,p}$ is the total collision force acting on the particle p, $\boldsymbol{F}_{d,p}$ is the drag force between the gas and the particle p, $\boldsymbol{F}_{b,p}$ is the buoyancy force, **n** is the unit normal to the direction of the total collisional force and R_p is the particle p radius.

The total collisional force acting on the generic particle p is computed by means of a soft-sphere approach[1]. According to this method, the collisions involving *p*th particle during a time step are first detected whenever particle *p* is overlapped with another one. Then, the collision force is computed for each detected collisional event as a function of the relative velocity and the magnitude of the overlap vector by means of a spring-slider-dashpot model[2] (Eq.(S3)-(S4)).

$$\boldsymbol{F_{ab,n}} = \left(-\boldsymbol{k_n}\boldsymbol{\delta_n^{\frac{3}{2}}} - \boldsymbol{\eta_n}\boldsymbol{v_{ab}}\cdot\boldsymbol{n_{ab}}\right)\boldsymbol{n_{ab}} \tag{S3}$$

$$\boldsymbol{F_{ab,t}} = \begin{cases} \boldsymbol{\mu_c}\left\|\boldsymbol{F_{ab,n}}\right\| & \left\|\boldsymbol{F_{ab,t}}\right\| > \boldsymbol{\mu_c}\left\|\boldsymbol{F_{ab,n}}\right\| \\ -\boldsymbol{k_t}\boldsymbol{\delta_t} - \boldsymbol{\eta_t}(\boldsymbol{v_{ab}} - (\boldsymbol{v_{ab}}\cdot\boldsymbol{n_{ab}})\boldsymbol{n_{ab}}) & \left\|\boldsymbol{F_{ab,t}}\right\| \leq \boldsymbol{\mu_c}\left\|\boldsymbol{F_{ab,n}}\right\| \end{cases} \tag{S4}$$

where $\boldsymbol{v}_{ab}$ is the relative velocity between the two colliding particles *a* and *b*, $\boldsymbol{n}_{ab}$ is the unit vector connecting the centers of *a* and *b*, μ_c is the friction factor of the slider and k and η are the spring stiffness and the damping coefficient of the dashpot which can be derived from the Young modulus E, the Poisson ratio ν and the restitution coefficient e of the particles as proposed in [2]. Subscripts n and t refer to the normal and tangential directions with respect to the plane normal to $\boldsymbol{n}_{ab}$.

Finally, each collisional force vector is summed up to obtain the total force vector acting on particle *p* at that specific time step.

The drag force (Eq.(S5)) is a function of a drag coefficient β computed by means of the Gidaspow model[3] (Eq.(S6)) and the relative velocity vector. In particular, the drag coefficient is a function of the magnitude of the relative velocity vector, the geometry of the particle and the gas fraction in the computational cell hosting the particle (ε_g), which is computed by means a Particle Centroid Method – PCM[4].

$$\boldsymbol{F_{d,p}} = V_p\beta\left(\boldsymbol{U_g} - \boldsymbol{v_p}\right) \tag{S5}$$

$$\beta = \begin{cases} \dfrac{150(1-\varepsilon_g)}{\varepsilon_g}\dfrac{\mu_g}{D_p^2} + 1.75\left(1-\varepsilon_g\right)\dfrac{\rho_g}{D_p}\left\|\boldsymbol{U_g} - \boldsymbol{v_p}\right\| & \epsilon < 0.8 \\ \dfrac{3}{4}C_D\dfrac{\rho_g}{D_p}\left\|\boldsymbol{U_g} - \boldsymbol{v_p}\right\|\varepsilon_g{}^{-1.65} & \epsilon \geq 0.8 \end{cases} \tag{S6}$$

where μ_g is the gas dynamic viscosity, D_p is the particle diameter, V_p is the volume of the particle, ρ_g is the density of the gas phase at the particle position, $\boldsymbol{U_g} - \boldsymbol{v_p}$ is the relative velocity between a generic particle p and the gas phase and C_D is evaluated according to Schiller and Neumann[5] (Eq.(S7)):

$$C_D = \begin{cases} 24[1 + 0.15(\varepsilon_g Re_p)^{0.687}]/(\varepsilon_g Re_p) & Re_p < 1000 \\ 0.44 & Re_p \geq 1000 \end{cases} \quad \textbf{(S7)}$$

where Re_p is the particle Reynolds number based on the magnitude of the particle-gas relative velocity vector.

The buoyancy force (Eq.(S8)) is computed as a function of the pressure gradient experienced by the gas surrounding the particle.

$$\boldsymbol{F}_{buoyancy} = V_p \nabla P \quad \textbf{(S8)}$$

The particle species mass (Eq.(S9)) and species sites (Eq.(S10))balances, describing the coupling between gas-particle transfer phenomena and catalytic reactions, result into the following ODE system:

$$\rho_{g,p} \varepsilon_p \frac{d\omega_{j,p}}{dt} = K_{c,j} S_{v,p} \rho \left(\omega_{j,g} - \omega_{j,p}\right) + \sum_{n=1}^{NR} \nu_{j,n} r_{n,p} MW_j \quad \textbf{(S9)}$$

$$\frac{d\theta_{j,p}}{dt} = \frac{R_{j,p}^{het}}{\sigma_{cat}} \quad \textbf{(S10)}$$

where ω_j, $K_{c,j}$, MW_j and $\nu_{j,n}$ are the mass fraction, the mass transfer coefficient, the molecular weight and the stoichiometry coefficient of the *n*th reaction of the *j*th species, ε_p is the porosity of the catalyst, $\rho_{g,p}$ is the average density of the perfect gas mixture in the catalyst and ρ is the mean density between the mixture in the catalyst and the gas. $\theta_{j,p}$ and $R_{j,p}^{het}$ are the coverage and the production rate due to heterogeneous reactions of the *j*th adsorbed species and σ_{cat} is the concentration of active sites on the catalytic surface.

The evaluation of the catalytic reaction rates is performed by means of the catalyticFOAM framework[6] and they are expressed on the basis of the mean surface molar concentration in the *p*th particle. Both microkinetic and rate equation models can be adopted for the description of the catalytic chemistry. In case of a microkinetic model, the reaction rates $r_{n,p}$ in the species mass balances are composed by only adsorption and desorption reactions. In case of rate equation kinetics, the site

balances are not solved and the reaction rates in the species mass balances represents the kinetics of the whole catalytic process by means of macro-reactions.

According to the hierarchy of the methodology chosen, i.e. Euler-Lagrange CFD-DEM, the gas-particle mass transfer is not quantified directly by means of the indefinite transport equations. Indeed, the computational cells are bigger than particles, thus the gas-particle interface is not described in detail. However, lower hierarchy DNS has proven the validity[7] of the empirical Gunn correlation[8] (Eq. (S11)) used to compute the interphase mass transfer coefficient $K_{c,j}$ in this work. In particular, the Gunn correlation (Eq.(S11)) has been used to compute the Sherwood Number, from which the gas-particle mass transfer coefficient has been derived.

$$Sh_j = \left(7 - 10\varepsilon_g + 5\varepsilon_g^2\right)\left(1 + 0.7Re_p^{0.2}Sc_j^{0.33}\right) + \left(1.33 - 2.4\varepsilon_g + 1.2\varepsilon_g^2\right)\mathrm{Re_p}^{0.7}Sc_j^{0.33} \quad \textbf{(S11)}$$

where Sc_j is the Schmidt Number related to species *j*.

1.2 Gas phase

Once the solid phase is updated, the gas-particle momentum and mass transfer contributions are computed for each particle in each cell. By doing so, the interphase momentum and mass source fields are computed and exploited into the gas governing equations (Eq.(S12)-(S14)), solved by means of a segregated approach and reported in the following:

$$\frac{\partial(\varepsilon_g\rho_g)}{\partial t} + \nabla\cdot\left(\varepsilon_g\rho_g\boldsymbol{U}_g\right) = 0 \quad \textbf{(S12)}$$

$$\frac{\partial(\varepsilon_g\rho_g\boldsymbol{U}_g)}{\partial t} + \nabla\cdot\left(\varepsilon_g\rho_g\boldsymbol{U}_g\boldsymbol{U}_g\right) = -\varepsilon_g\nabla P - \nabla\cdot\left(\varepsilon_g\bar{\bar{\boldsymbol{\tau}}}\right) + \varepsilon_g\rho_g\boldsymbol{g} + \boldsymbol{S}_U \quad \textbf{(S13)}$$

$$\frac{\partial(\varepsilon_g\rho_g\omega_{j,g})}{\partial t} + \nabla\cdot\left(\varepsilon_g\rho_g\boldsymbol{U}_g\omega_{j,g}\right) = -\nabla\cdot\left(\varepsilon_g\rho_g\Gamma_j\nabla\omega_{j,g}\right) + R_j^{hom} + \boldsymbol{S}_{\omega_j} \quad \textbf{(S14)}$$

where $\boldsymbol{U}_g$ is the gas velocity, P is the pressure, **g** is the gravity vector, $\boldsymbol{S}_U$ refers to the gas-solid momentum transfer and $\bar{\bar{\boldsymbol{\tau}}}$ is the Newtonian stress tensor. Γ_j, R_j^{hom} and $\boldsymbol{S}_{\omega_j}$ are the mixture diffusivity, the production rate due to the homogeneous reactions in the gas phase and the gas-solid mass tranfer of the *j*th species. The evaluation of homogeneous reaction rates is performed by means of

openSMOKE++ framework[9]. Nevertheless, they have not been accounted for in this work. The energy balances are implemented in the framework and illustrated in our previous paper[10]. However, they are not herein reported since only isothermal simulations has been performed in this work.

2 Computational domain and numerical methods

The meshes used in the simulation of the small test reactor and the million-particle lab scale reactor simulations are herein described along with the numerical methods employed.

2.1 Test Reactor

Fig. S.1 shows the computational domain employed for the test reactor.

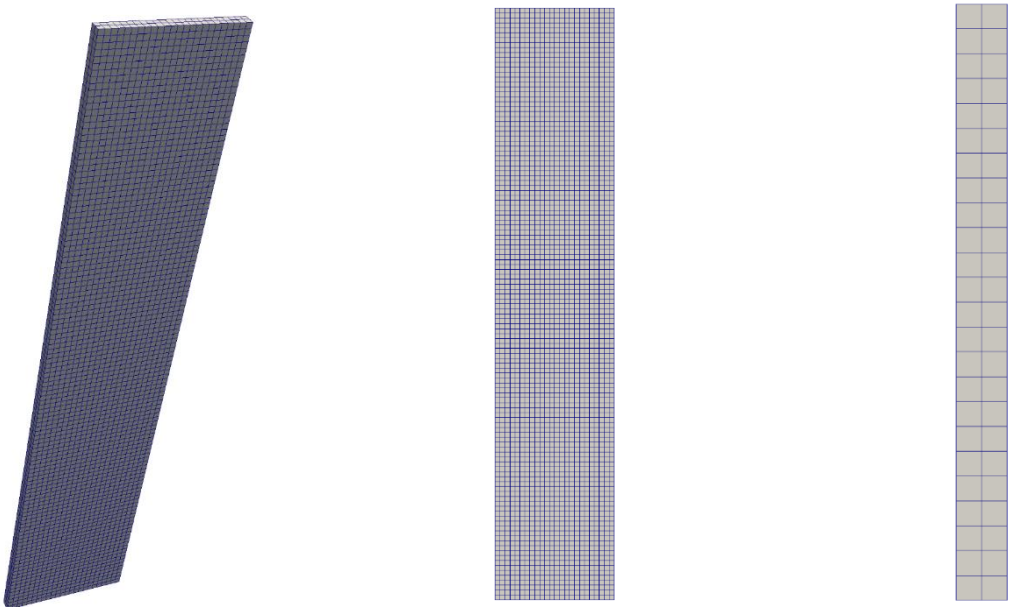

a) **b)** **c)**

Figure S.1. Computational grid adopted for the simulation of the methanation and steam reforming test reactors: 3D view (a), section parallel to the flow (b) and section normal to the flow (c)

It consists of 5760 cells distributed as follows: 24 cells along the width, 120 cells along the height and 2 along the depth. The mesh consists of hexahedra and it is perfectly orthogonal.

Pressure-Implicit with Splitting of Operators (PISO) loop with 3 pressure correctors and no non-orthogonal corrections is employed to solve the pressure-velocity coupling.

The discretization schemes available in the OpenFOAM framework have been used. Among these schemes, the gradient operator has been discretized with the *cellLimited Gauss linear* scheme, the

divergence operator with the second order *Gauss LimitedLinear* scheme and the *Gauss Linear Corrected* scheme for Laplacian operator. A forward Euler scheme is employed for the temporal discretization.

2.2 Million-Particle Lab Scale Reactor

Fig. S.2 shows the computational domain employed for the lab scale reactor.

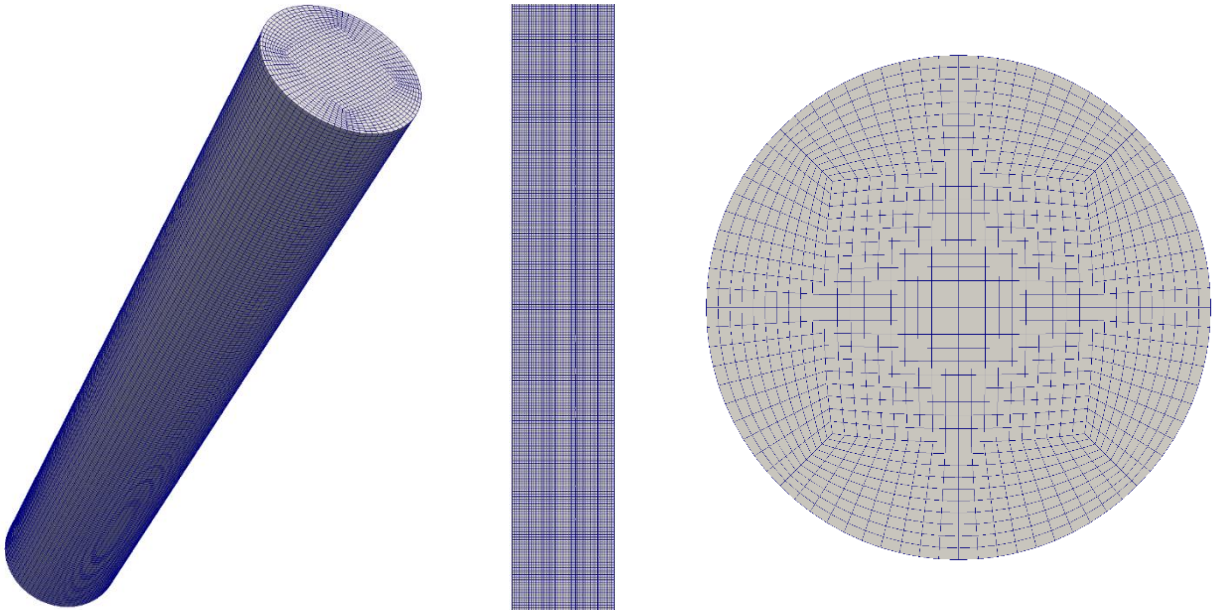

a) **b)** **c)**

Figure S.2. Computational grid adopted for the simulation of the methanation million particle reactor: 3D view (a), section parallel to the flow (b) and section normal to the flow (c)

It consists of 288,000 cells where 20 cells are along the radius while 258 cells along the height. The mesh has a maximum non-orthogonality of 29 (average 6) and a maximum skewness factor of 1.02. A PISO loop with 3 pressure correctors has been used to solve the pressure-velocity coupling. Non-orthogonal corrections are not used due to the low degree of non-orthogonality (i.e. < 40).

The discretization schemes available in the OpenFOAM framework have been used. Among these schemes, the gradient operator has been discretized with the *cellLimited Gauss linear* scheme, the divergence operator with the second order *Gauss LimitedLinear* scheme and the *Gauss Linear Corrected* scheme for Laplacian operator. A forward Euler scheme is employed for the temporal discretization.

3 Parametrical analysis of the effect of $y_{i,min}$

The variable normalization is carried out according to a logarithmic scale as reported in Eq. (2) in the manuscript. In this case, it is necessary to define a value of $y_{i,min}$ when the actual minimum value of the variable is equal to zero, to avoid numerical issues with the logarithm. In this view, the selected value of $y_{i,min}$ might affect the results of the binning procedure and eventually the accuracy of the Particle Agglomeration techniques. Hereby, different values of $y_{i,min}$ have been tested in the test reactor to assess the effect on the simulation results. Three different values, i.e. 10^{-5}, 10^{-15} and 10^{-20}, has been tested. Fig. S.3 shows the average mass fractions in the bed for different $y_{i,min}$. A negligible effect of the minimum value is observed when a sufficiently small value (< 10^{-5}) is considered.

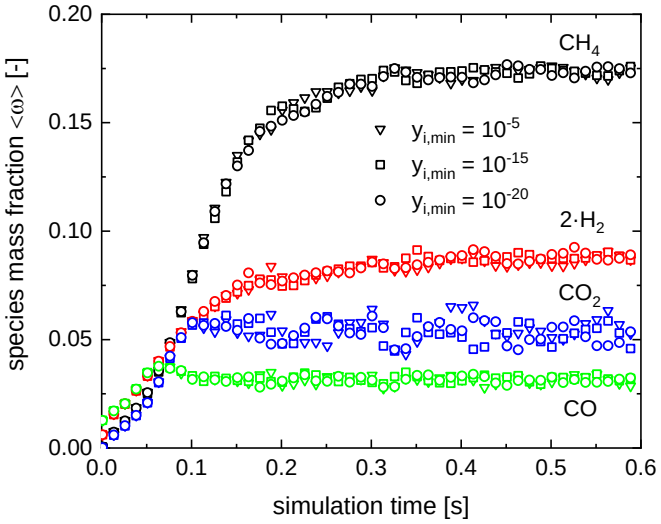

Figure S.3. Species mass fraction for the methanation system along the test reactor evaluated by using the CP & PA algorithm for different values of the $y_{i,min}$

References

1. Cundall, P. A. & Strack, O. D. L. A discrete numerical model for granular assemblies. *Géotechnique* **29**, 47–65 (1979).
2. Tsuji, Y., Tanaka, T. & Ishida, T. Lagrangian numerical simulation of plug flow of cohesionless particles in a horizontal pipe. *Powder Technol.* **71**, 239–250 (1992).

3. Gidaspow, D. *Multiphase flow and fluidization : continuum and kinetic theory descriptions*. (Academic Press, 1994).

4. Norouzi, H. R., Zarghami, R., Sotudeh-Gharebagh, R. & Mostoufi, N. *Coupled CFD-DEM Modeling: Formulation, Implementation and Application to Multiphase Flows*. *Coupled CFD-DEM Modeling: Formulation, Implementation and Application to Multiphase Flows* (2016). doi:10.1002/9781119005315

5. Schiller, L. & Naumann, Z. A drag coefficient correlation. *Z.Ver.Deutsch.Ing* **77**, 318–320 (1933).

6. Maestri, M. & Cuoci, A. Coupling CFD with detailed microkinetic modeling in heterogeneous catalysis. *Chem. Eng. Sci.* **96**, 106–117 (2013).

7. Tavassoli, H., Peters, E. A. J. F. & Kuipers, J. A. M. Direct numerical simulation of non-isothermal flow through dense bidisperse random arrays of spheres. *Powder Technol.* **314**, 291–298 (2017).

8. Gunn, D. J. Transfer of heat or mass to particles in fixed and fluidised beds. *Int. J. Heat Mass Transf.* **21**, 467–476 (1978).

9. Cuoci, A., Frassoldati, A., Faravelli, T. & Ranzi, E. OpenSMOKE++: An object-oriented framework for the numerical modeling of reactive systems with detailed kinetic mechanisms. *Comput. Phys. Commun.* **192**, 237–264 (2015).

10. Uglietti, R., Bracconi, M. & Maestri, M. Coupling CFD-DEM and microkinetic modeling of surface chemistry for the simulation of catalytic fluidized systems. *React. Chem. Eng.* **3**, 527–539 (2018).